3rd 2017 NASL
3rd North American Symposium on Landslides
June 4-8 2017, Roanoke, Virginia, USA

Forensic rockfall scar analysis: Development of a mechanically correct model of rockfall failure

de Vilder, S.J., s.j.de-vilder@durham.ac.uk, Rosser, N.J., n.j.rosser@durham.ac.uk, Brain, M.J., matthew.brain@durham.ac.uk, Vann Jones (nee Norman), E.C., e.c.vann-jones@durham.ac.uk
Department of Geography, Durham University, Durham, DH1 3LE, United Kingdom

ABSTRACT: The mechanical controls on small (< 10 m³), individual rockfall in jointed rock masses are not well constrained. We use forensic analysis of rockfall detachment surfaces (scars) which display fractured surfaces broken through intact rock, termed rock bridges as well as pre-existing discontinuities, to understand failure mechanisms. The relative significance of intact rock fracture versus release along pre-existing surfaces in stability has not been thoroughly investigated using field data. The relative role of each of these components determines where weakening, is important in controlling the nature and timing of rockfall. This is vital for defining mechanically accurate models of failure.
An initial inventory of rockfall scars from coastal rock cliffs was captured using high-resolution gigapixel imaging and terrestrial laser scanning to determine these relationships. Fracture mapping, planar surface identification, and weathering classification were undertaken to identify similarities in the mechanical controls on failure. Preliminary analysis reveals that even small rockfall display a multi-stage failure history, whereby final failure occurs through fracture of a single unweathered rock-bridge. Intact rock breakage accounts for 22 ±12% of the full scar surface. The rock bridges are commonly clustered at the scar crest or base, while planar pre-existing joint surfaces dominate the scar center. This suggests that although cantilevered, most rockfalls in this inventory are more likely to fail through tension. We consider volumetric and lithologic controls on failure mode, and consider the wider potential of this approach.

INTRODUCTION

Rockfall scars contain valuable information that describes the controls on failure mode. Scars are commonly characterized by a combination of discontinuity surfaces of varying persistence and zones of relatively fresh fracturing through previously intact rock, with both being subjected to varying degrees of weathering (Fig. 1). These zones of fractured intact rock are referred to as rock bridges throughout this paper. Previous research has shown that failure occurs through progressive fracturing of intact rock bridges, in a process termed step-path failure (Jennings, 1970; Scavia, 1995; Eberhardt et al., 2004; Kemeny, 2005; Brideau et al., 2009). A wide variety of research has been conducted to understand the kinematics, rock mass characteristics and driving forces of failure, yet few studies have tried to link this understanding to evidence recorded in the remaining rockfall scar, and in particular the role of intact rock fracture that may be suitable for verifying slope stability model assumptions. Rock bridges contribute substantially to the stability of a slope (Scavia, 1990; Frayssines & Hantz, 2009; Paronuzzi & Sera, 2009; Paronuzzi

et al., 2016), with various modelling studies highlighting that scars that display 0.1% of breakage through rock across the failure surface greatly increases the overall factor of safety (Jennings, 1970; Frayssines & Hantz, 2009; Elmo et al., 2011). Therefore, the prevalence of rock bridges within failure surfaces must be an important control on stability. Conceptually, the location and distribution of rock bridges within a scar is suggested to control failure mode (Stock et al., 2011; Tuckey & Stead, 2016). As these zones are critical for stability, rock bridge weakening driven by weathering or stress changes due to progressive failure, can be a temporal constraint on failure (Eberhardt et al., 2004; Gischig et al., 2011; Viles, 2013). It is vital to properly understand the presence, characteristics and role of these zones in order to construct mechanically correct models of rockfalls.

Few studies have mapped rockfall scars to examine their characteristics in detail, and these studies have been limited to single event cases –notably studies of large scale rockfalls (10 m^3 to 10,000 m^3) (Paronuzzi & Sera, 2009; Lévy et al., 2010; Stock et al., 2011; Stock et al., 2012; Paronuzzi et al., 2016) or small inventories of similar scale rockfalls (Frayssines & Hantz, 2006). These studies display percentage estimates of rock bridge area within the total failure surface, which range from 0.2% to 30% and contain qualitative information regarding the other scar characteristics. Discontinuity persistence has also been used to predict the presence of rock bridges within jointed rock masses and provides percentage estimates of length of intact rock along a particular discontinuity set (Sturzenegger & Stead, 2012; Grøneng et al., 2009; Matasci et al., 2015; Tuckey & Stead, 2016; Karami et al., 2007).

These estimates display rock bridge proportions of 1 % to 5 %. Modelling studies using discrete fracture networks (DFN's) have shown via back analysis that rock bridges often account for 3 % to 45 % of a final failure surface (Elmo et al., 2007; Karami et al., 2007; Moffit et al., 2007; Elmo et al., 2011; Gischig et al,. 2011a), with the higher percentage in fracturing due to some discontinuity sets having a much higher proportion of intact rock along their length than other discontinuity sets.

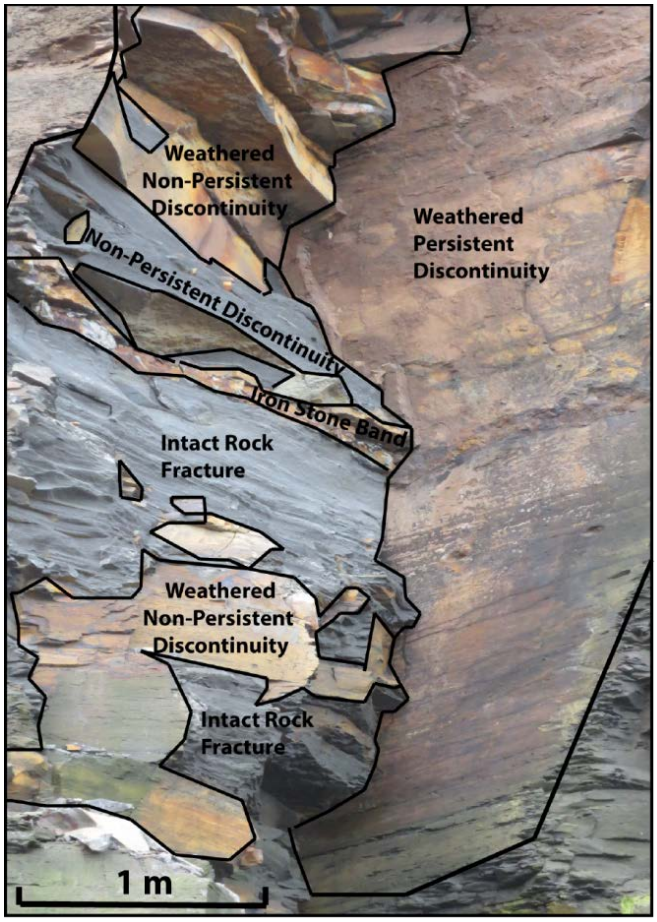

Figure 1. Photograph of a recent rockfall scar from the Staithes coastline. This shale scar displays weathered discontinuities of varying persistence, unweathered discontinuity surfaces, and fresh breakage of intact rock.

However, most of these studies provide little or only qualitative information on the exact details of rock bridges, discontinuity surfaces or weathering within rockfall scars, and their relative significance. This includes their location within the scar, and their size and distribution. The variation in weathering has not been quantified or linked to factors including joint continuity or intact rock strength degradation. As Stock et al. (2011) and Bonilla-Sierra et al. (2015) infer, the location of a rock bridge is important for understanding if rockfall fails in tension or shear, as they can form a pivot point about which the failing rock block is able to potentially rotate and fail in tension (Fig. 2). Therefore, not only does the proportion of intact rock fracture and discontinuity surfaces need to be defined, their characteristics are also important controls on failure.

This paper presents the results of forensic analysis using an inventory of rockfall scars observed using high resolution 3D scanning and imaging along the coastal cliffs of Staithes, North Yorkshire, UK. This database is examined to consider how the characteristics of weathering, rock bridges and planar joint surfaces can be used to infer controls on rockfall failure.

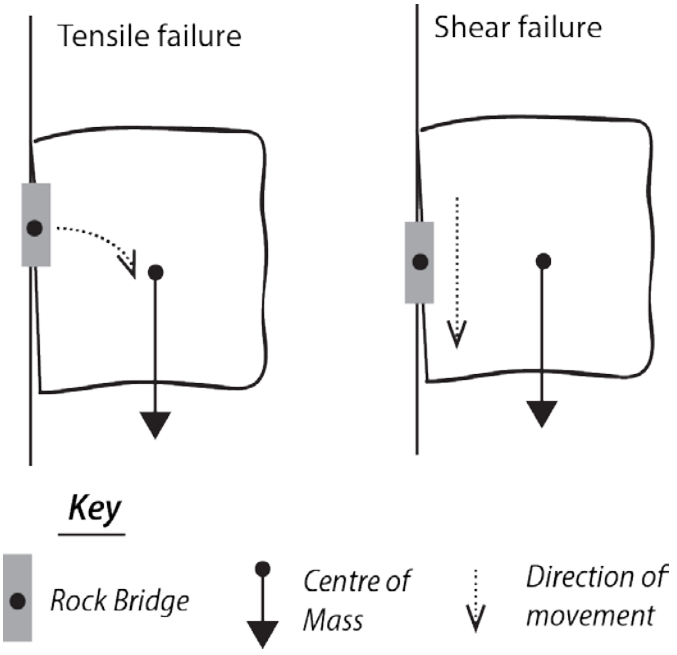

Figure 2: Rock bridge location may determine failure mode via influencing the balance of mass within an incipient rockfall failure. Tensile failure may occur when the rock bridge location deviates from the center of mass, creating a mass imbalance and the potential for rotation. Conversely, shear failure occurs when the rock bridge and rockfall center of mass are balanced.

STUDY SITE

Rockfall scars were recorded from a 200 m long section of coastal cliffs located between Staithes and Boulby, as shown in Figure 3. The cliffs are near vertical and up to 60 m in height, with a wide shore platform which extends >300 m seawards at low tides. This is a storm-dominated coastline, which experiences a semi-diurnal tide of c. 6 m. The cliffs are comprised of a lower and upper shale unit, and an interbedded siltstones and sandstones unit, which form part of the Lower Jurassic Redcar Mudstone and Staithes Sandstone formations, and are all capped by a layer of glacial till (Rawson and Wright, 2000). All these layers display a bedding dip of 2° to the south east, and a complex discontinuity pattern which varies in persistence between the different rock type exposures. The lower shale unit is characterized by widely spaced persistent joints, and has a surface covering of algae as it sits within the tidal range zone. In contrast the upper shale unit displays a less persistent joint pattern, and in places the rock mass appears to be massively jointed. The interbedded siltstone and sandstones comprise beds of up to 3 m in thickness, which displays a blocky weathered discontinuity pattern with dilated joints. Norman (2012) showed that of the rockfalls recorded along this section of cliff over a 2 year period, 60 % of net eroded volume was related to rockfalls between 0.1 m^3 and 10 m^3, accounting for >20 % of rockfalls recorded. Rockfalls of this size are important for coastal erosion and retreat.

Previous research along this coast has also shown that rockfalls occur across the whole cliff face, not just within the wave inundation zone, with higher numbers of failures concentrated in certain lithological layers (such as the interbedded siltstones & sandstones) as well as at the boundaries between layers (Lim et al., 2010; Rosser et al., 2013). The different lithological units in part control rockfall geometry, which indicates that the rock mass structure and jointing patterns of the cliff face determine failure volume and shape (Lim et al., 2010). However, pure kinematic failure – without any fracturing through rock bridges, is not a dominant failure mechanism along these cliffs, with many rockfall scars, such as seen in Figure 1, displaying rock bridges in combination with discontinuity release surfaces (Rosser et al., 2013).

METHODS

Data Collection

3D point clouds were captured monthly using a Reigl VZ – 1000 terrestrial laser scanner (TLS). The scans were collected from one scan positon located at a distance of 100 m from the cliff toe, and the resulting point clouds covered a 200 m long section of cliff, with a 0.01 m to 0.02 m point spacing. Change detection was undertaken on the sequential scans using the methodologies outlined in Rosser et al. (2005), and provided the locations

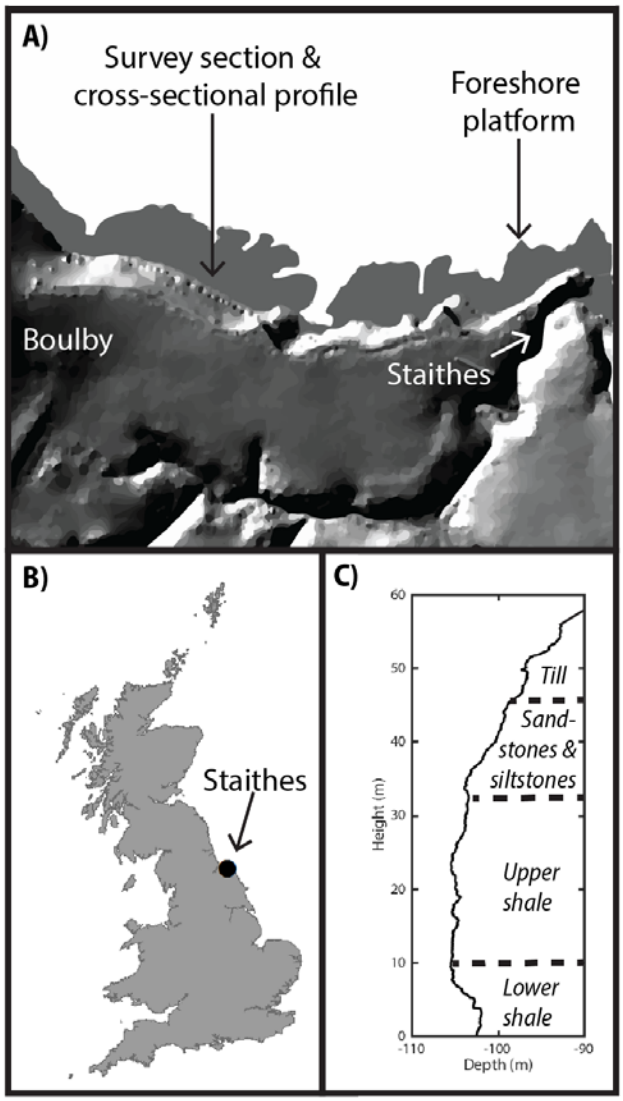

Figure 3. A) Location of the 100 m survey section between Boulby and Staithes. B) Location of Staithes along the North Yorkshire coast, UK. C) Cross-section profile displaying the different lithological layers present within the survey section.

of rockfalls and their characteristics within the scan area.

To provide textural and color information of the rockfall scar surfaces, Gigapixel photographic imagery was collected. A Gigapan Epic Pro was used in conjunction with a 50MP Canon EOS 5DS R and a 300 mm telephoto lens to capture multiple images of the cliff face (c. 150 individual photographs). Associated Gigapan Stitch software was used to sequence and stitch the photos into one resulting gigapixel panoramic image, with an average file size of 4 GB. The photographs were collected from the same position as the TLS, with each individual photograph achieving an on cliff pixel resolution of 1 mm to 2 mm. Aperture, shutter speed and ISO were manually adjusted to allow for sharp high-quality images to be captured.

The panoramic pictures were geo-referenced onto the DEM model of the cliff face derived from the 3D point clouds, using a spline transformation in ArcMap 10.2. This required the manual selection of >200 control points to allow the 2D image to be stretched into place over the 3D DEM. From this, the resulting rockfall scars were 'clipped' from the panoramic photograph using the rockfall locations determined from change detection (Fig. 4).

Obtaining both high-resolution point clouds and imagery allows the fine scale detail of the shape of the rockfall scars themselves (in terms of point cloud change detection) and the texture of fracturing (on scales greater than 2 mm) within the rockfall scar as well as subtle color differentiation.

Rockfall Scar Mapping

Fifteen rockfall scars were chosen to form the preliminary database considered here. These rockfalls were chosen to cover a range of volumes (from 0.02 m^3 to 27 m^3) and the three dominant exposed lithologies (lower shale, upper shale, and interbedded siltstones & sandstones) present within this section of cliff (Fig. 3). The features of the rockfall scars were mapped and separated into three categories; fractures/edges, planar surfaces, and weathered surfaces. Edges are representative of fracturing through intact rock and as such form a component part of a broken rock bridge. Mapping allows qualitatively determined zones of high - concentrations of edges to be defined. These high concentrations are representative of broken rock bridges (Fig. 5a.). Rock bridge proportion is calculated as a percentage of the total scar surface area, and herein referred to as *% rb*. A planar surface was considered indicative of pre-existing (pre-failure) joints and bedding faces, with a 'smooth' texture and limited fracturing evident.

Each individual planar surface within a rockfall scar was mapped, with the number of planar surfaces per scar, their total area and location within the rockfall scar noted (Fig. 5b.). Their orientation and resulting geometry (i.e. wedge or planar shaped) was also recorded. Weathering classification was based on color differential

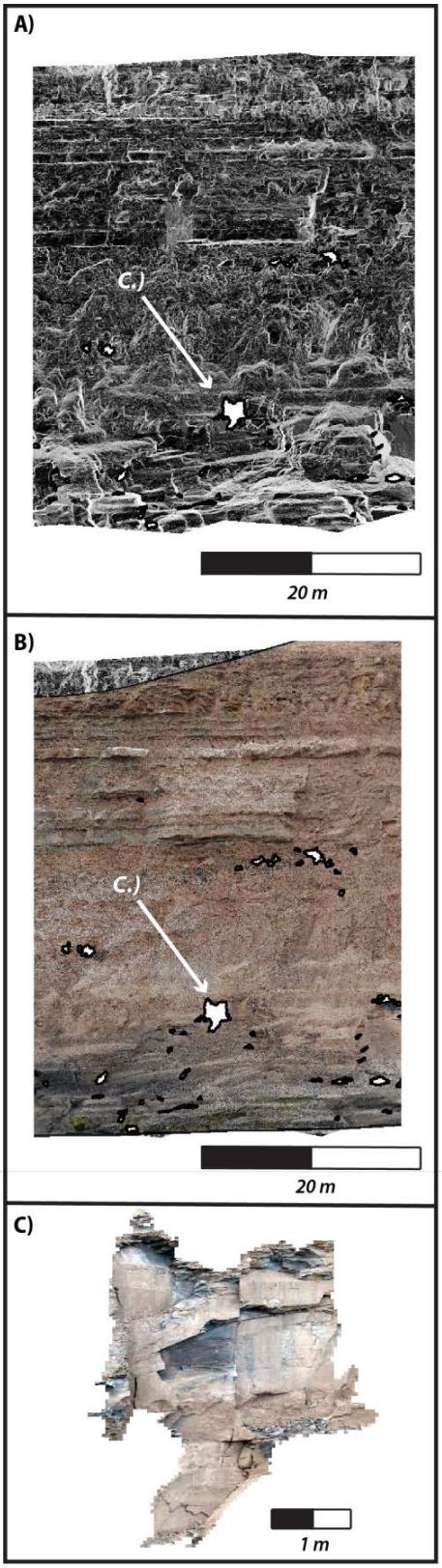

Figure 4. A) DEM of the scan area, display rockfalls greater than > 0.1 m². B) DEM with gigapixel panoramic image stretched onto it. C) The rockfall 'clipped' out of the gigapixel image using the DEM derived rockfall locations and geometries.

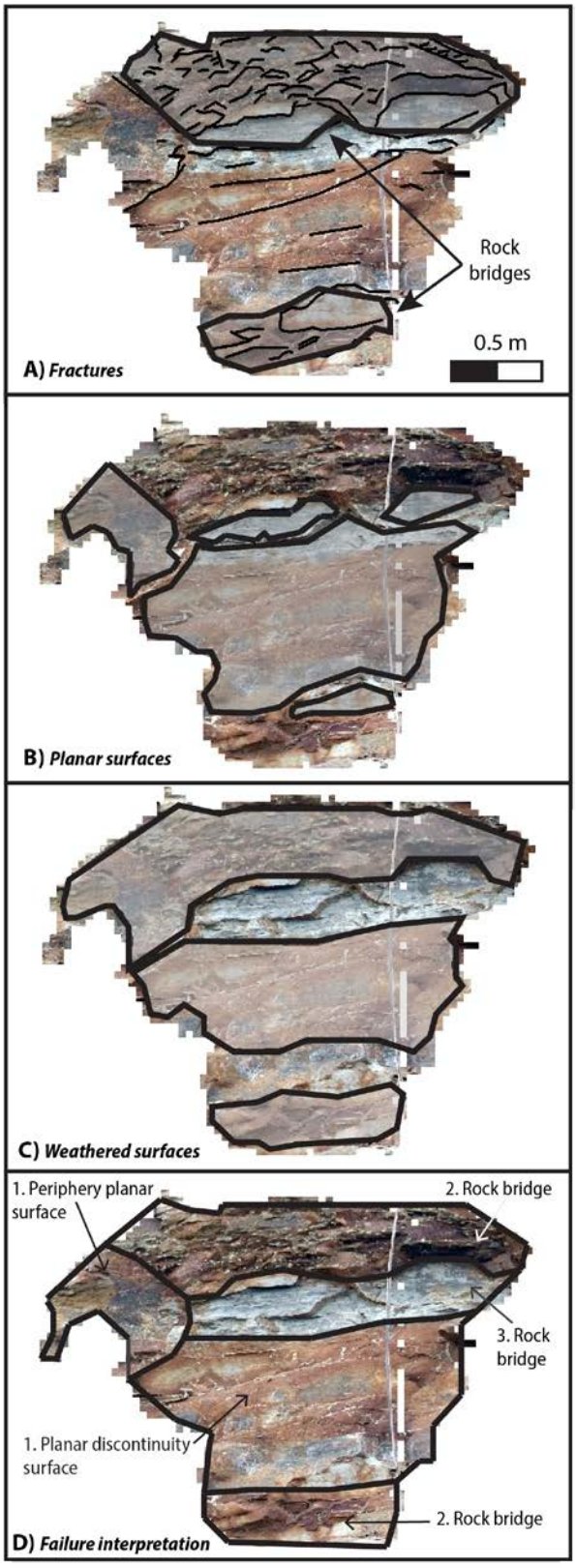

Figure 5. A) Mapped edges with fracture zones B) Mapped planar surfaces, C) Mapped weathered surfaces and D) Interpretation of failure mechanisms in rockfall scar, with the numbers (1 to 3) representing the stages of failure.

relative to the overall cliff face, with the total area of weathered surfaces, and their location recorded within the scar (Fig. 5c.). Both planar surface (*% ps*) and weathered proportions (*% w*) were also calculated as percentages of total failure surface.

Table 1 presents the information recorded from each of the rockfall scars. From this information for each rockfall scar, an interpretation of failure sequence and associated controls was constructed, as displayed in Figure 5d. This example rockfall scar will be used to illustrate how an interpretation was undertaken. This failure scar is comprised of multiple rock bridges and discontinuity surfaces which display a varying degree of weathering, and have subsequently been separated into three stages of failure. The weathered planar surface (Fig. 5d - 1.) forms the majority of the rockfall scar with a planar surface on the periphery. Fracturing has occurred through two rock bridges located at the base and top of scar (Fig. 5d - 2.). As these two zones are weathered, it is hypothesized that this fracturing occurred before final failure. Final failure occurred after fracturing through an unweathered rock bridge (Fig. 5d - 3.) located at the top of the scar. The time between failure of the first and last rock bridge is unknown, but must have been substantial enough to allow for significant weathering of the fractured surface.

DATABASE ANALYSIS

Proportion of rock bridges & discontinuity faces

The proportion of rock bridges (*% rb*), planar surfaces (*% ps*) and weathering (*% w*) was calculated from the database (Table 2). Rock bridges account for approximately 20% of failure surface area, but can range from 7% up to nearly half of the failure surface. Planar discontinuity surfaces found within the rockfall scar account for 50% of failure area on average, and also display a wide range from 30% to 75% of failure surface.

Weathered surfaces account for 40% of rockfall scar area, and show the largest range, with weathering occurring both along discontinuity faces as well as previously failed rock bridges. This can be determined from comparing the location of weathering with those of rock bridges and planar surfaces in Table 1, as well as from the interpretation of failure sequence (see: Fig. 5d). The *% rb* values are higher than previously observed in rockfall scars, with a previous range of 0.2% to 26%, with a mean of 4% and standard deviation of 7% (Frayssines & Hantz, 2006; Paronuzzi & Sera, 2009; Lévy et al,. 2010; Stock et al., 2011; Paronuzzi et al., 2016). This may be due to differences in mapping rock bridge areas, with previous studies characterization on color and texture with unweathered surfaces defined as rock bridges. As shown in Figure 5d, rock bridges can be broken through, and weathered, before final failure of the rockfall. As a result, it may be that the *% rb* within a slope has been underestimated. This dataset (n = 15) along with previously published studies (n *= 17)* represent a wide range of lithologic and rock mass strength settings generating rockfalls that display 6 orders of magnitude difference in volume (from 0.02 m^3 to 10,000 m^3). This variation may result in different rockfall scar characteristics.

Rock bridge characteristics

The number of planar surfaces and rock bridges increase with increasing rockfall scar surface area (see Fig. 6a). This linear relationship indicates that for approximately 1 m^2 area of a failure surface there is at least 1 rock bridge, with an average area of c. 0.2 m^2. Analysis of individual rock bridge area confirms this relationship (Fig. 6b) This empirical estimate could be extrapolated to the whole slope, and this number used to feed into discrete fracture network (DFN) models of slope stability (Moffit et al., 2007; Elmo et al., 2011; Tuckey and Stead, 2016). However, no information is provided on the location of these rock bridges with respect to discontinuity surfaces, or failure scar geometry. The percentage of rock bridges along a particular discontinuity set can control failure evolution, especially if the orientation of that set is critical for global stability of the slope (Elmo et al., 2011; Gischig et al., 2011a; Stead & Wolter, 2015; Tuckey & Stead, 2016).

An increase in the number of rock bridges also means that for failure to occur, for larger rockfalls fracturing through multiple intact rock bridges is required. Figure 7 illustrates this increasing complexity of failure history for rockfall of increasing size. Nearly all of the rockfalls, irrespective of volume, displayed a multi-stage

Table 1: Rockfall scar database of 15 rockfall scars containing information relating to rock bridges, planar joint surfaces and weathering.

ID	Date	Area (m^2)	Vol (m^3)	Lithology	Rock bridge proportion (*% rb*)	No. of rock bridge zones	Rock bridge location*	Planar surface proportion (*% ps*)	No. of planar surfaces	Planar surface location*	Weathered Proportion (*% w*)	Weathered Location*	Shape
1***	Mar-16	0.11	0.02	Lower Shale	18	1	T (LS)	64	1	T, M, B	0	NA	Planar
2	Mar-16	0.11	0.03	Upper Shale	36	2	T, B	57	4	M	38	M	Wedge
3	Mar-16	0.15	0.02	Siltstone	7	1	M	76	5	T, M, B	80	T, M, B	Wedge
4	Mar-16	0.15	0.03	Lower Shale	13	1	T,M (LS&RS), B	53	4	M	39	B (LS)	Planar
5	Mar-16	0.43	0.11	Lower Shale	21	1	M (LS)	58	5	M (RS)	30	M (LS)	Arch
6	Mar-16	0.45	0.07	Siltstone	7	2	NA	67	1	T, M, B	56	T, B	Planar
7**	Mar-16	0.88	0.52	Lower Shale	14	2	M	48	4	T, M (LS & RS), B	20	T, M (LS & RS), B	Wedge
8	Aug-15	1.01	0.2	Lower Shale	13	2	T, B	73	3	T, M, B	85	T, M, B	Planar
9	Jan-16	1.81	0.35	Siltstone	43	3	T, B	29	5	T, M	66	T, M, B	Planar
10	Oct-15	2.56	1.24	Lower Shale	8	3	M	55	3	M, B	6	T, B	Wedge
11***	Aug-15	3.34	1.07	Siltstone	.42	2	T, B	51	5	M	65	T, M, B	Planar
12	Nov-15	4.09	2.12	Upper Shale	39	3	M (LS), B (LS)	47	1	M (RS)	19	M	Planar
13	Aug-15	4.8	2.01	Upper Shale	35	2	T, B	44	9	M	13	T	Planar
14***	Aug-15	6.37	3.04	Lower Shale	18	9	T, M	44	14	M (LS)	4	T, M (LS)	Arch
15	Jan-16	26.9	27	Siltstone	19	30	T, B	32	32	M & B	45	T, B	Planar

* Location abbreviations: T = top, M= middle, B = base, LS = left side, RS = right side.
** Rockfall displayed in Figure 4
*** Rockfalls displayed in Figure 6.

Table 2: Descriptive statistics of the proportion of each element within a rockfall scar.

	Mean	Standard Deviation	Min	Max
Rock bridge proportion (*% rb*)	22.15	12.76	6.67	43.09
Planar surface proportion (*% ps*)	53.09	13.06	28.95	76
Weathered proportion (*% w*)	37.77	26.93	0	85.15

failure history (Table 1). As the example rockfall scar in Figure 5 shows, the temporal evolution of these scars is complex as the rockfall appears to have stabilized between the first fracture through a rock bridge and the final rock bridge failure, long enough for surface weathering to occur. Further investigation of failure sequence may provide useful information on the role of damage accumulation through time within a rockslope.

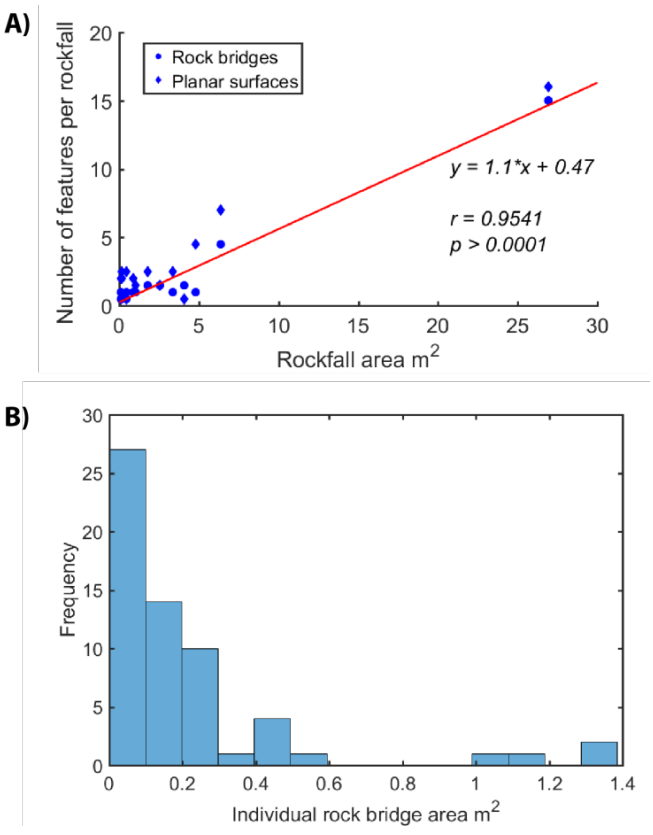

Figure 6. A) Scatter plot showing as rockfall size increases the number of rock bridges and planar surfaces (i.e. joint faces) also increases. B) Histogram of individual rock bridge area, with most rock bridges ≤ 0.3 m².

Rock bridge location

Analysis of fracture zone locations reveals that rock bridges are mainly located at either the top or base of rockfall scars. The few cases in which rock bridges are located in the middle of the scar are associated with wedge shaped failures (Table 1), whereby rock bridges are located at the intersection of the discontinuities forming the wedge. The reverse pattern is observed for planar surfaces, with most flat scar surfaces located in the middle of the footprint.

Therefore, rockfalls from these cliffs are suspended or 'hang' from the rock slope prior to failure. This has implications for failure mode as Stock et al. (2011) inferred in their case-study of rockfalls in Yosemite, USA.

Modelling has shown that greater tensile cracking is associated with rock bridges located at the top of failure surface, while shear cracking is associated with rock bridges located in the center or lower parts of the failure surface (Bonilla-Sierra et al., 2015). The amount and distribution of tensile or shear cracking is dependent on the center of gravity of a failing mass, the depth of the failure surface, and the moment generated prior to release. In this case, tensile-associated flexural or rotational failures are likely to be the dominant mode of failure, unless a wedge shape failure mode is predominant (Paronuzzi & Sera, 2009; Paronuzzi et al., 2016).

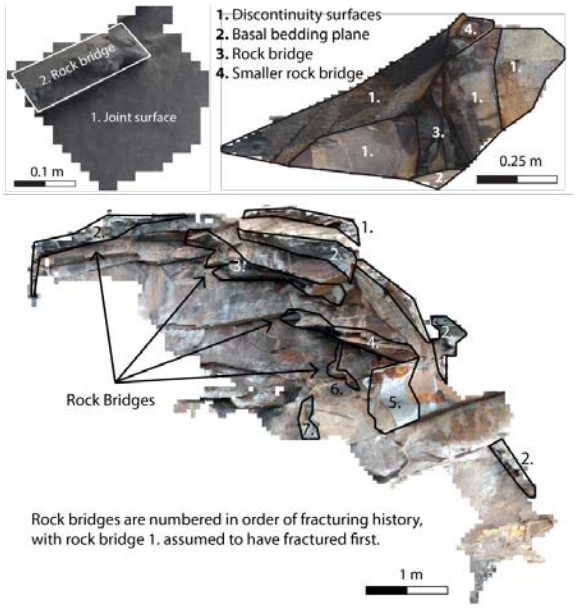

Figure 7: Three rockfall scars and their interpretations are presented. With increasing area, the number of rock bridges and discontinuity surfaces increases, as does the stages required for failure.

Need for a larger database

All of these observations and their implications are based on a dataset of *n = 15*, and combining with previously published data this in total consists of 32 rockfalls for which rockfall scar analysis has been undertaken. As stated earlier, these 32 rockfalls consist of a wide variation in rock mass structure, lithology (i.e. granite, limestone, siltstone, and shale), and volume (0.02 m^3 to 10,000 m^3). To determine the appropriate sample size for this database of rockfalls recorded along the North Yorkshire coastline, the sample needed for accurate representation of rockfall area and volume, plus rock bridge area, planar surface area and weathered surface area within the rockfall scar were determined. These attributes were chosen as they are the key variables from which *% rb*, *% ps*, and *% w* are calculated, and therefore will affect the statistical distribution and significance of these values. For example, a margin of error of 0.25 m^2 (as defined in Table 3) for the mean rock bridge area of 0.81 m (using the mean rockfall area), will generate a variance in *% rb* from 16 % to 30 % ,with a range just greater than that of the expected standard deviation from mean *% rb* (Table 2). The use of the same margin of error for planar and weathered surfaces generated similar results. Table 3 outlines that a sample size of greater than 100 rockfall scars is needed for 90 % degree of confidence in results, while to achieve a 99 % degree of confidence in the mean value of the population 200 to a 1000 rockfall scars are required using the given margin of errors. As such, the relationships and values determined earlier in this paper have to be treated with caution.

This small sample size does not allow the whole population of rockfall scars to be accurately characterized, nor does it allow for the role of lithology, area or slope geometry to be determined. Determination of these sample sizes (Table 3) does not also take into account that the cliffs are composed of three lithologies and their associated structure. Thus, to ascertain if there are statistically significant differences between the different rock masses a much larger database is need. On the whole, to obtain statistically significant values of the characteristics of rock bridges for empirical inputs into slope stability models, analysis of a larger database of rockfall scars is required. More information is needed about rockfall geometry, failure depth and slope angle to allow for the classification of failure mode and controls on rockfall failure to be established.

Table 3. Sample size determination of rockfall area and scar characteristics.

	Area (m^2)	Rock bridge area (m^2)	Planar Surface area (m^2)	Weathered surface area (m^2)
Margin of error	*1*	*0.25*	*0.25*	*0.25*
90% (z0.05)	115.24	70.33	187.23	385.65
95% (z0.025)	163.60	99.84	265.80	547.49
99% (z0.005)	282.59	172.47	459.12	945.71

FUTURE WORK

The creation of larger more comprehensive rockfall scar database (> 300 rockfall scars) requires a different methodological approach. The mapping by hand of a such a large number of rockfall scars is time-consuming and inefficient, plus allows for qualitative judgement calls on what constitutes a rock bridge, and weathered surface. A semi-automatic classification approach of forensic scar analysis of both rock bridges (and thus discontinuity faces) and weathered surfaces are needed. The next stage of this project will be the development of these methods and analysis of the subsequent rockfall scar database. It is proposed that for mapping of fractures and texture of the rockfall scar surface, edge detection based on the classification of pixel value range will be used (based upon Li et al., 2008). In this method, edges are determined as areas where there is a significant contrast in pixel values across a specified distance. From the ‘edge’ maps, zones of higher density will be classified as rock bridges. Automatic weathering classification will be based on pre-defined color pixel values and ranges, which is then applied to the whole dataset, in order to ensure consistency. In addition to these two methods, information on rockfall geometry and associated center of gravity, along with failure slope angle will be used to assess and test models of the dominant failure mode for these rockfalls. Information about failure surface orientation with respect to rock bridge location will ascertain which discontinuity sets and associated rock bridges are

critical for slope stability. This database will enable statistically significant relationships concerning rock bridge and weathering proportion within failure to be determined, as well as the contributions of both to failure mode and stresses acting on the slope. It will provide increased information about controls on rockfall evolution and failure.

CONCLUSIONS

This paper presents an initial database of 15 rockfall scars observed and analyzed along the coastal cliffs of North Yorkshire. Mapping of the scars has allowed the proportion and characteristics of rock bridges, discontinuities and weathering to be determined. Analysis of this information has revealed:

- Rock bridges account for approximately 22 % ±12% of rockfall scar area, and weathered surfaces account for 40 % ±26 %
- The number of rock bridges and discontinuity faces (i.e. joints or bedding) increases linearly with increasing rockfall area, and hence volume. This implies that on average, for every 1 m² of rockfall failure area there is 1 rock bridge.
- Nearly all rockfall display multi-stage failure histories, whereby prior to final failure several stages of fracturing can occur through intact rock bridges. The scale of complexity of rockfall scar surfaces increases with rockfall volume.
- Rock bridges are predominately located at the top and/or base of the scar, with this location possibly an important control on mode of failure, and the associated strength parameter critical for stability.
- The analysis of the samples in this study (and all other previous rockfall scar case-studies) is small, yet covers a wide range of variables such as rockfall volume, lithology and rock mass characteristics. In addition, the relationships derived are largely qualitative. Statistical analysis has shown that to have a greater degree of confidence (> 99%) in the results and relationships determined from them, a database of greater than 300 rockfall scars is needed.

ACKNOWLEDGEMENTS

Ongoing support for this research is provided by ICL Fertilizers (UK) Ltd.

REFERENCES

Bonilla-Sierra, V., Scholtès, L., Victor, F., and Elmouttie, M., 2015, DEM analysis of rock bridges and the contribution to rock slope stability in the case of translational sliding failures: International Journal Rock Mechanics Mining Sciences, Vol. 80, pp.67–78.

Brideau, M., Yan, M., and Stead, D., 2009, The role of tectonic damage and brittle rock fracture in the development of large rock slope failures: Geomorphology, Vol. 103, pp.30–49.

Eberhardt, E., Stead, D., and Coggan, J.S., 2004, Numerical analysis of initiation and progressive failure in natural rock slopes-The 1991 Randa rockslide: International Journal Rock Mechanics Mining Sciences, Vol. 41, pp.69–87.

Elmo, D., Clayton, C., Rogers, S., Beddoes, R., and Greer, S., 2011, Numerical Simulations of Potential Rock Bridge Failure within a Naturally Fractured Rock Mass. In: Eberhardt, E. and Stead, D. (Editors), Slope Stability 2011: International symposium on rock slope stability in open pit mining and civil engineering, Vancouver, Canada, pp 1–13.

Elmo, D., Yan, M., Stead, D., and Rogers, S.F., 2007, The importance of intact rock bridges in the stability of high rock slopes - towards a quantitative investigation using an integrated numerical modelling; discrete fracture network approach. In: Potvin, Y. (Editor), Slope Stability 2007 : Proceedings of the 2007 International symposium on rock slope stability in open pit mining and civil engineering, Perth, Australia, pp 253–266.

Frayssines, M., and Hantz, D., 2006, Failure mechanisms and triggering factors in calcareous cliffs of the Subalpine Ranges (French Alps): Engineering Geology, Vol. 86, pp. 256–270.

Frayssines, M., and Hantz, D., 2009, Modelling and back-analysing failures in steep limestone cliffs: International Journal Rock Mechanics Mining Sciences, Vol. 46, pp. 1115–1123.

Gischig, V., Amann, F., Moore, J.R., Loew, S., Eisenbeiss, H., and Stempfhuber, W., 2011a, Composite rock slope kinematics at the current Randa instability, Switzerland, based on remote sensing and numerical modeling: Engineering Geology, Vol. 118, pp. 37–53.

Gischig, V., Moore, J.R., Evans, K., Amann, F., and Loew, S. 2011b, Thermomechanical forcing of deep rock slope deformation : 1. Conceptual study of a simplified slope: Journal Geophysical Research, Vol. 116, No.F04010, pp. 1-18.

Grøneng, G., Nilsen, B., and Sandven, R., 2009, Shear strength estimation forAknes sliding area in western Norway: International Journal Rock Mechanics Mining Sciences, Vol. 46, pp. 479–488.

Jennings,J.E., 1970, A mathematical theory for the calculation of the stability of open cast mines. In: Van Rensburg, P. (Editor), Planning open pit mines: Proceedings of the Symposium on the Theoritical background to the planning of open pit mines with special reference to slope stability, Johannesburg, South Africa, pp 87–102.

Karami, A., Greer, S., and Beddoes, R., 2007, Numerical assessment of step-path failure of northwest wall of A154 Pit, Diavik Diamond Mines. In: Potvin, Y. (Editor), Slope Stability 2007 : Proceedings of the 2007 International symposium on rock slope stability in open pit mining and civil engineering, Perth, Australia, pp 293–305

Kemeny, J., 2005, Time-dependent drift degradation due to the progressive failure of rock bridges along discontinuities: International Journal of Rock Mechanics and Mining Sciences: Vol.42, pp.35–46.
Lévy. C., Baillet, L., Jongmans, D., Mourot, P., and Hantz, D., 2010, Dynamic response of the Chamousset rock column (Western Alps, France): Journal Geophysical Research, Vol. 115, No.F04043, pp.1–13.
Li, Y., Onasch, C.M., and Guo, Y., 2008, GIS-based detection of grain boundaries: Journal Structural Geology, Vol. 30, pp.431–443.
Lim, M., Rosser, N.J., Allison, R.J., and Petley, D.N., 2010, Erosional processes in the hard rock coastal cliffs at Staithes, North Yorkshire: Geomorphology, Vol. 114, pp.12–21.
Matasci, B., Jaboyedoff, M., Loye, A., Pedrazzini, A., Derron, M.H., and Pedrozzi, G., 2015, Impacts of fracturing patterns on the rockfall susceptibility and erosion rate of stratified limestone: Geomorphology, Vol. 241, pp.83–97.
Moffit, K., Rogers, S., and Beddoes, R., 2007, Analysis of slope stability in strong, fractured rock at the Diavik Diamond Mine, NWT. In: Eberhardt, E. Stead, D. and Morrison, T. (Editors), Rock Mechanics: Meeting Society's challenges and Demands, Proceedings of the 1st Canada-US Rock Mechanics Symposium, Vancouver, Canada, pp 1245–1250
Norman, E.C., 2012, Microseismic monitoring of the controls on coastal rock cliff erosion. Unpublished Ph.D. Thesis, Department of Geography, Durham, Durham University, U.K., 259 p.
Paronuzzi, P., and Sera, W., 2009, Stress state analysis of a collapsed overhanging rock slab : A case study: Engineering Geology, Vol. 108, pp.65–75.
Paronuzzi, P., Bolla, A., and Rigo, E., 2016, 3D Stress – Strain Analysis of a Failed Limestone Wedge Influenced by an Intact Rock Bridge: Rock Mechanics Rock Engineering, Vol. 49, pp.3223–3242.
Rawson, P.F., and Wright, J.K., 2000, The Yorkshire Coast - 3rd edition: Geologists'Association, London, U.K., 130 p.
Rosser, N.J., Brain, M.J., Petley, D.N., Lim, M., and Norman, E.C., 2013, Coastline retreat via progressive failure of rocky coastal cliffs: Geology, Vol. 41, pp. 939–942.

Rosser, N.J., Petley, D.N., Lim, M., Dunning, S.A., and Allison, R.J., 2005, Terrestrial laser scanning for monitoring the process of hard rock coastal cliff erosion: Quarterly Journal Engineering Geology Hydrogeology, Vol. 38, pp. 363–375.
Scavia, C., 1990, Fracture mechanics approach to stability analysis of rock slopes: Engineering Fracture Mechanics, Vol. 35, pp. 899–910.
Scavia, C., 1995, A method for the study of crack propagation in rock structures: Geotechnique, Vol. 45, pp.447–463.
Stead, D., and Wolter, A., 2015, A critical review of rock slope failure mechanisms : The importance of structural geology: Journal Structural Geology, Vol. 74, pp.1–23.
Stock, G.M., Bawden, G.W., Green, J.K., Hanson, E., Downing, G., Collins, B.D., Bond, S., and Leslar, M., 2011, High-resolution three-dimensional imaging and analysis of rock falls in Yosemite Valley, California: Geosphere, Vol. 7, pp.573–581.
Stock, G.M., Martel, S.J., Collins, B.D., and Harp, E.L., 2012, Progressive failure of sheeted rock slopes: the 2009-2010 Rhombus Wall rock falls in Yosemite Valley, California, USA: Earth Surface Processes and Landforms, Vol. 37, pp. 546–561.
Sturzenegger, M., and Stead, D., 2012, The Palliser Rockslide, Canadian Rocky Mountains : Characterization and modeling of a stepped failure surface: Geomorphology, Vol. 138, pp.145–161.
Tuckey, Z., and Stead, D., 2016, Improvements to fi eld and remote sensing methods for mapping discontinuity persistence and intact rock bridges in rock slopes: Engineering Geology, Vol. 208, pp. 136–153.
Viles, H.A., 2013, Linking weathering and rock slope instability: non-linear perspectives: Earth Surface Processes Landforms, Vol. 38, pp. 62–70.